Manifestation of Rossby Waves in the Global Magnetic Field of the Sun during Cycles 21–24

Irina A. Bilenko

Moscow M.V. Lomonosov State University, Sternberg Astronomical Institute, Moscow, 119234, Univercitetsky pr. 13, Russia; bilenko@sai.msu.ru

Abstract

The evolution of the solar global magnetic field (GMF) was investigated and compared with oscillations of different periods during cycles 21–24. The data from the Wilcox Solar Observatory were used. The results indicate that GMF structures were associated with certain oscillations. Oscillations of 81.83–163.65 days were associated with structures lasting 10–20 CRs. They occurred as some pulses during solar maxima. Oscillations of 163.652–463.680 days were associated with GMF structures lasting ≈20–50 CRs. They match two peaks in the magnetic-field cycle. Oscillations of 1.270–5.231 yr were formed during the dominance of the sectorial GMF structure. Oscillations of 5.231–13.451 yr were the most intense. From cycle 22 to 24, their intensity decreased, and the range of periods narrowed and shifted to longer periods, determining the corresponding changes in the oscillations of 81.83 days–5.231 yr and associated GMF structures. They match well the evolution of the zonal GMF structure. They are assumed to be a descending part of a period of ≈⩾60 yr. A decrease in the magnetic field from cycle 22 to 24 may be due to a decrease in the intensity of these oscillations. Some periodicities of the revealed oscillations are in good agreement with the estimates of the periods for fast magnetic Rossby waves. The GMF structure connection with Rossby waves is discussed.

Unified Astronomy Thesaurus concepts: Solar cycle (1487); Solar oscillations (1515); Solar magnetic fields (1503); Solar photosphere (1518); Wavelet analysis (1918)

1. Introduction

The solar global magnetic field (GMF) is manifested in the large-scale magnetic fields at the photosphere and the global changes in their systematic patterns (Levine 1977; Hoeksema & Scherrer 1988; Hoeksema 1991), in the changes in the solar corona during solar cycles (Mackay & Yeates 2012), in the polar field reversals, in coronal hole time-spatial evolution (Wang & Sheeley 1994; Bilenko & Tavastsherna 2016), in the evolution of the low-order spherical harmonics of the PFSS decomposition of the solar magnetic fields (Knaack & Stenflo 2005), and in the evolution of the interplanetary magnetic field (Wilcox 1967; Levine 1979). Solar GMF affects space weather and geomagnetic activity (Ponyavin 2004). The evolution of GMF determines the conditions for eruptive events, such as flares, coronal mass ejections, and prominence eruptions (Mordvinov et al. 2002; Svalgaard et al. 2011; Bilenko 2012, 2013, 2014).

Currently, the physical processes that lead to the formation, the observed time-spatial distribution, and the cycle evolution of large-scale photospheric magnetic fields and that in the solar interior are not yet well understood. An interesting hypothesis is that solar magnetic fields can be induced by Rossby waves generated around a thin magnetized layer at the bottom of the convection zone (Gilman 1969a, 1969b). Theoretical studies have shown the possibility of generating Rossby waves of various scales in a tachocline (Zaqarashvili 2018; Gachechiladze et al. 2019; Raphaldini et al. 2019). Zaqarashvili et al. (2007) showed that the magnetic field causes the splitting of low-order Rossby waves into fast and slow magnetic Rossby waves. The fast magnetic Rossby mode corresponds to ordinary hydrodynamic Rossby waves. Slow magnetic Rossby waves can modulate the dynamo magnetic field and consequently long-term variations and the strength of solar cycles (Zaqarashvili et al. 2015; Gurgenashvili et al. 2016). The

simulation performed by Tikhomolov & Mordvinov (1996) shows that Rossby vortices can be generated within a thin layer beneath the convection zone as a result of heating from the solar interior and deformation of the lower boundary of the convection zone, and that they lead to the observed large-scale magnetic-field structures.

The manifestation of Rossby waves has been revealed in various phenomena of solar activity: in sunspots (Zaqarashvili et al. 2015; Gurgenashvili et al. 2016), in magnetic field and sunspot indices (Feng et al. 2017), radio flux at a frequency of 2800 MHz (Mei et al. 2018), in the evolution of bright points (McIntosh et al. 2017), and in the rate and parameters of flares, CMEs, and prominences (Lou 2000; Lou et al. 2003; Bilenko 2013, 2014). The signature of Rossby waves was found in the solar photosphere (Kuhn et al. 2000; Knaack et al. 2005). Global-scale equatorial Rossby waves are thought to be an essential component of solar internal dynamics (Löptien et al. 2018; Liang et al. 2019). Sturrock et al. (2013) found the neutrino periodicities, which may be attributed to r-mode oscillations in the tachocline. Silva & Lopes (2017) suggested that solar Rossby waves can partly influence some phenomena in the Earth's atmosphere with periods close to Rieger-type periodicity.

The goal of the paper is to investigate spatiotemporal evolution of the GMF and its relationship with the oscillations of Rossby wave periods during solar cycles 21–24.

2. Data

Data on the solar mean magnetic field (the magnetic field of the Sun as a star), synoptic maps of the observed large-scale photospheric and calculated magnetic fields on the source surface were provided by the Wilcox Solar Observatory for cycles 21–24 (years 1976–2018, Carrington rotations (CRs) 1642–2212). The source-surface magnetic field is calculated from the photospheric fields using a potential field model
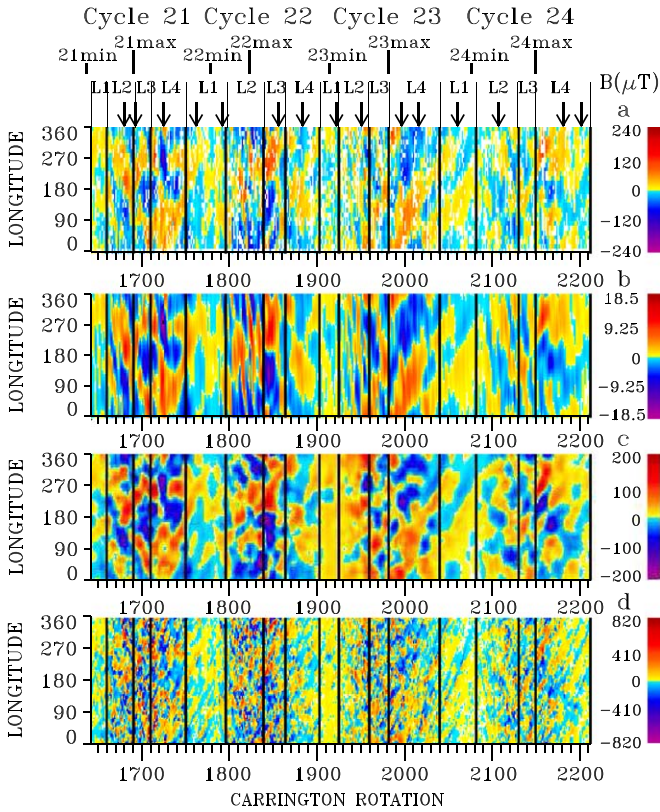
Figure 1. Longitudinal diagrams: (a) magnetic field of the Sun as a star, (b) source-surface magnetic field, (c) large-scale photospheric magnetic fields smoothed by a nine-datum point window, and (d) large-scale photospheric magnetic field. Yellow–red denotes positive-polarity magnetic fields and blue–lilac denotes negative-polarity magnetic fields.

(Altschuler & Newkirk 1969; Schatten et al. 1969; Altschuler et al. 1977; Hoeksema 1984) with the source-surface location at 2.5 $R_\odot$. The $R_\odot = 2.5$ radial model data were used.

3. Solar GMF Cycle Evolution

To analyze the time-spatial evolution of the solar GMF, time-longitude diagrams of the strength and polarity of the magnetic field calculated at the source surface (Figure 1(b)), observed large-scale photospheric magnetic field (Figure 1(d)), and that smoothed with a nine-datum point window (Figure 1(c)) were created (Bilenko 2014; Bilenko & Tavastsherna 2016). To create the *BMF* diagram (Figure 1(a)), for each CR (*x*-axis), the value of the mean magnetic field was set in accordance with the longitude of the central meridian for each day of the CR (*y*-axis), because about half the contribution to the mean magnetic field comes from the center 35% of the disk area (Scherrer et al. 1977). Each vertical bar represents the latitude-averaged longitudinal distribution of positive- (yellow–red) and negative-polarity (blue–lilac) magnetic fields within a given CR. In each diagram, the *x*-axis denotes the date of 0° CR longitude at the central meridian and the *y*-axis denotes longitude. In Figures 1–4, vertical lines and shadows, indicate the long-lived structures L1–L4 ($\approx$20–50 CRs). The arrows indicate transitions between some GMF structures with a shorter lifetime ($\approx$10–20 CRs). Cycle maxima and minima based on the 13-month smoothed monthly sunspot number time series are marked at the top.[1]
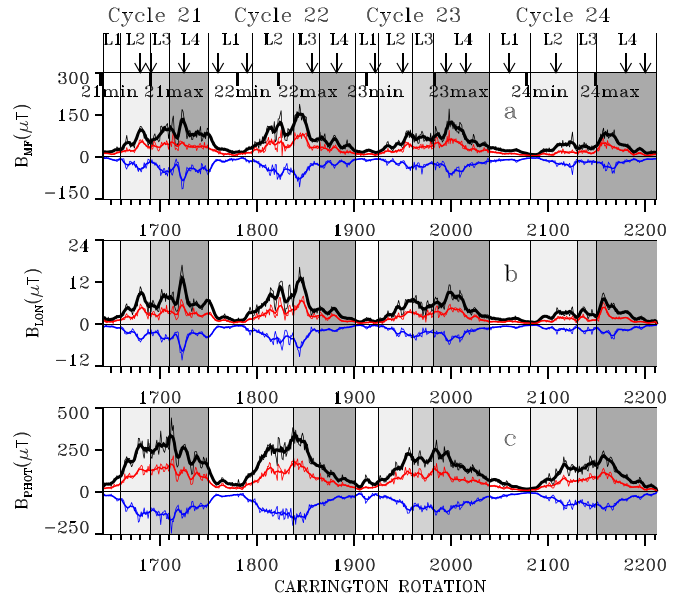

Figure 2. Variations of the CR-averaged (thin lines) and seven CR-averaged (thick lines) positive- and negative-polarity magnetic fields and the sum of their absolute values (black lines): (a) mean magnetic field (*BMF*), (b) calculated source-surface magnetic field (*BLON*), and (c) large-scale photospheric magnetic fields (*BPHOT*).
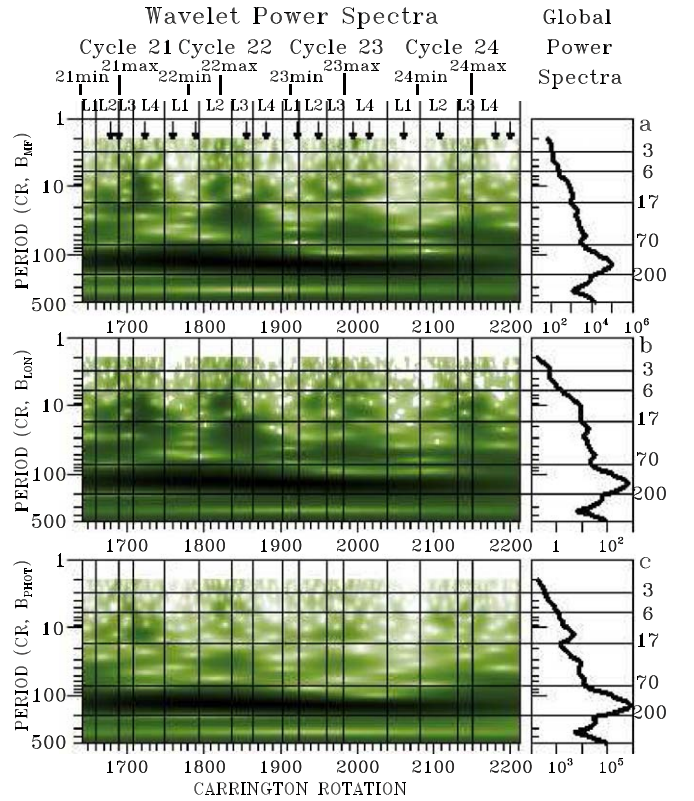

Figure 3. Wavelet spectra: (a) *BMF*, (b) *BLON*, and (c) *BPHOT*.

Figure 2(a) shows the strength of the observed mean magnetic fields of positive and negative polarity averaged over one CR (thin lines) and seven CRs (thick lines) and the sum of their moduli (*BMF*). Those derived from the longitudinal diagrams in Figures 1(b) and (d) are presented in Figures 2(b) (*BLON*) and (c) (*BPHOT*). The GMF structure is purely visible in photospheric magnetic fields due to local magnetic fields of
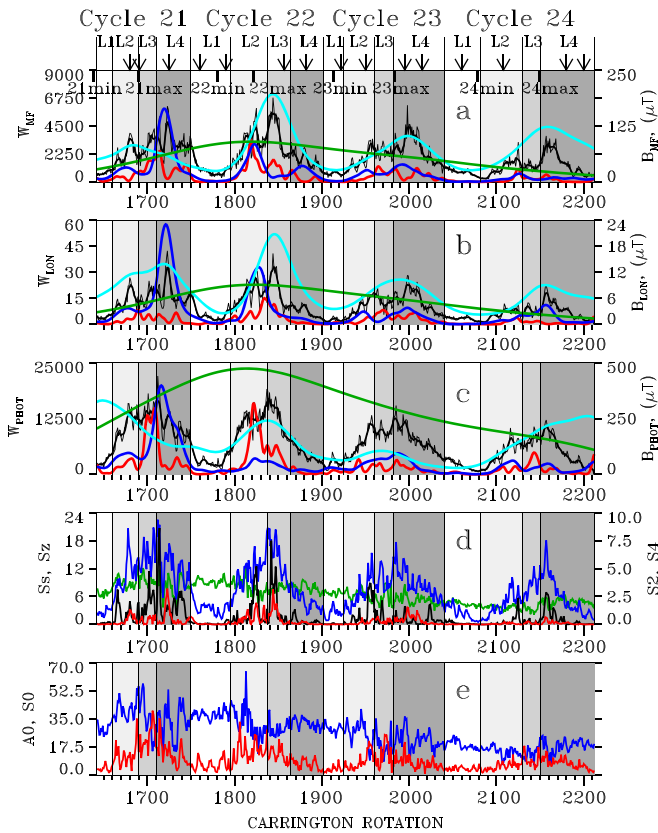
Figure 4. (a)–(c) Mean intensity of the oscillation periods *P1*, *P2*, *P3*, and *P4* from wavelet spectra with superimposed moduli of the corresponding magnetic field (black lines): (a) *WMF*, (b) *WLON*, and (c) *WPHOT*. Red denotes *P1* × 3, blue denotes *P2*, light blue denotes *P3*, and green denotes *P4*/20. (d) Sum of sectorial (blue line) and zonal (green line) harmonics, *S2* (red line), and *S4* (black line) sectorial harmonics. (e) *A0* (blue line) and *S0* (red line).

active regions, but the structure becomes more pronounced in the smoothed diagram.

Magnetic fields of positive and negative polarity were concentrated at fixed longitudinal intervals, forming the structure of the GMF. The structure was more pronounced at latitudes from −55° to 55° (Bilenko & Tavastsherna 2016). The time–space distribution of structures depended on the phase of a cycle. During solar minima, structures were less intense. At the rising phases, the GMF structures increased in size and became more complex (Bilenko 2014). They formed large bipolar structures with strong magnetic fields persisting for as long as 2-3 yr during the maximum and early declining phases. At the late declining phases, some structures could exist longer, e.g., from 2002 to 2010 in cycle 23. The magnetic-field strength was the highest in cycle 22 and lowest in cycle 24. The magnetic-field strength increased to the cycle maximum in the form of some pulses. The number of pulses varied from three to six in different cycles, but the two largest peaks averaged over seven CR values in each cycle. Each pulse could be associated with the structure both in the observed and in the calculated magnetic field. The transition from one structure to another, due to the emergence of a new magnetic flux, occurred in a wide latitudinal range for one to three CRs (Bilenko & Tavastsherna 2016). The magnetic-field strength increases toward the center of a structure, but there may be several increases/decreases in long-lived structures. The correlation between the sum of the absolute values of *BMF* and *BLON* reached 0.917 (0.867 for positive- and 0.879 for negative-polarity

magnetic fields), and with the sum of the absolute values of *BPHOT* it was 0.812 (0.772 for positive- and 0.755 for negative-polarity magnetic fields).

4. Rossby-type Periodicities in the GMF

The wavelet analysis was used to decompose the one-dimensional CR-averaged moduli of the *BMF*, *BLON*, and *BPHOT* series into a two-dimensional time-period space (Figures 3(a)–(c)). Power is given in arbitrary units. It can be seen that the oscillations were packed into the period groups: 3–6 CRs (*P1*, 0.224–0.448 yr, 81.83–163.65 days), 6–17 CRs (*P2*, 0.448–1.270 yr, 163.652–463.680 days), 17–70 CRs (*P3*, 1.270–5.231 yr, 463.680–1909.27 days), and 70–200 CRs (*P4*, 5.231–14.945 yr). Time variations of the mean intensity of the selected wave intervals (between the horizontal lines in Figure 3) are presented in Figures 4(a)–(c). As each interval includes a number of periodicities, the evolution of the intensity of an individual periodicity may differ from that of the mean of the selected interval.

The geometric structure of the GMF can be described by the spherical harmonic analysis technique (Altschuler et al. 1975, 1977). Each harmonic, determined by its indices (n, m), represents the contribution of a particular geometric structure to the overall distribution of the solar field. Various harmonic power spectra can be calculated (Altschuler et al. 1977; Levine 1977) using

$$S_n = \sum_{m=0}^{n} [(g_n^m)^2 + (h_n^m)^2].$$

The coefficients g_n^m and h_n^m are determined using a method based on the orthogonality of the spherical functions (Hoeksema 1984). The purely latitudinal GMF structure (zonal) is described by harmonics with the $m = 0$. These harmonics describe the dynamics of axisymmetric components of the solar GMF. When $n = m$ the functions and structure of GMF are called sectorial. The sums of sectorial (*Ss*) and zonal (*Sz*, green line) harmonics are presented in Figure 4(d). Sectorial harmonics revealed the same variations as the magnetic field in each cycle. The correlation of *BMF*, *BLON*, and *BPHOT* with *Ss* was 0.801, 0.795, and 0.961. Figure 4(d) shows the sectorial harmonics *S2* ($n = m = 2$) and *S4* ($n = m = 4$). Figure 4(e) presents the sum of the axisymmetric, and with respect to the equator antisymmetric (*A0*), and symmetric (*S0*) harmonics (Stix 1977):

$$A0 = \sum_{n=1,3,\dots,9} (n + 1)g_n^0 P_n(\theta),$$

$$S0 = \sum_{n=2,4,\dots,8} (n + 1)g_n^0 P_n(\theta),$$

where $P_n^m(\theta)$ are the associated Legendre polynomials. The sum of *A0* was maximum when the zonal structure dominated at the minimum, and *S0* was maximal during the sectorial structure domination at the maximum of solar activity. The correlation of the *BMF*, *BLON*, and *BPHOT* with *S0* was 0.532, 0.522, and 0.668.

From Figures 3 and 4 it follows that the oscillations *P4* had the highest intensity. For example, for *BMF*, *P4* maximum intensity was approximately 9, 11, and 58 times higher than that of *P3*, *P2*, and *P1*. To present the periods *P1*–*P4* on the same graph the intensity of *P1* was multiplied by 3, and that of *P4* was divided by 20. The maximum intensity of *P4* was in the

growth phase of cycle 22 and the minimum was in the decline phase of cycle 24. During cycle 22, the oscillations ranged from 70 to 180 CRs (5.231–13.451 yr) and by cycle 24 the maximum intensity range narrowed and shifted to longer periods of ≈120–200 CRs (8.967–14.945 yr). The decrease in the intensity of $P4$ was probably the cause of the decrease in magnetic field from cycle 22 to 24. The wave is proposed to be a half of a period of ≈⩾60 yr. The oscillations showed a good correlation of $P4_{MF}$, $P4_{LON}$, and $P4_{PHOT}$ with the zonal GMF structure (0.588, 0.584, and 0.683) and $A0$ (0.528, 0.525, and 0.617). They include an 11 yr cycle of solar activity. Structures $L1$ were associated with periods of the zonal GMF structure domination during solar minima.

Oscillations $P1$–$P3$ formed some "packages" of periods that were similar and appeared during the sectorial structure domination in each cycle. Oscillations $P3$ were formed during the domination of the sectorial GMF structure. The correlation of intensities of $P3_{MF}$, $P3_{LON}$, and $P3_{PHOT}$ with Ss was 0.588, 0.777, and 0.286. Their intensity was high during strong cycles 21 and 22 and lower in weak cycles 23 and 24, following that of $P4$. The range of $P3$ intensity maximum shifted from 30–60 CRs (2.242–4.484 yr, 818.259–1636.52 days) in cycle 21, to shorter periods 17–50 CRs (1.270–3.736 yr, 463.680–1363.76 days) in cycle 22, and then to longer periods, 30–70 CRs (2.242–5.231 yr, 818.259–1909.27 days) in cycle 24. From this range the period of 1 yr was found in coronal bright points (McIntosh et al. 2017). They detected a retrograde phase speed of the wave, which corresponds to fast magneto-Rossby waves (Gachechiladze et al. 2019). Knaack et al. (2005), analyzing time series of longitudinally-averaged synoptic maps (NSO/ Kitt Peak) from 1975 to 2003, found a period of 1.8 yr located at latitudes ≈20°S–25°S, occurring in the total flux mainly from 1997 to 2003, which may be related to a possible r-mode signature in the photosphere with $m \approx 50$.

Oscillations $P2$ were associated with the GMF structures $L2$ and $L4$. They corresponded to two peaks in the magnetic field at the cycle maximum. Their intensity decreased from cycle 21 to 24. The correlation of $P2_{MF}$, $P2_{LON}$, and $P2_{PHOT}$ with Ss was 0.516, 0.574, and 0.552. During the transition from GMF structures $L2$ to $L3$ the oscillations disappeared simultaneously with the $L2$. During the lifetime of $L2$ structures, the intensity of the $S0$ components increased, while that of $A0$ decreased. They became equal during the $L3$ ($L2$ in cycle 22) structures. In cycles 23 and 24, the $L3$ structures coincided with a decrease in the magnetic field at the maximum. Oscillations of $P2$ reappeared again with the formation of the $L4$ structures. Their intensity decreased with decreasing magnetic field in $L4$ and they disappeared simultaneously with the $L4$ structures in each cycle. The correlation of $P2_{MF}$, $P2_{LON}$, and $P2_{PHOT}$ with $S0$ was 0.446, 0.452, and 0.474. During the $L4$ structures, both $S0$ and $A0$ decreased. In cycle 23, the sectorial components had a long "tail" and the $L4$ structure was the longest. These oscillations match the evolution of $S2$ and $S4$. Correlation of $P2_{MF}$, $P2_{LON}$, and $P2_{PHOT}$ with $S2$ ($S4$) was 0.477 (0.396), 0.525 (0.426), and 0.373 (0.459). For the midrange periodicities in solar radio flux at 2800 MHz and sunspot areas from 1947 February 1 to 2016 September 30, Mei et al. (2018) found that periodicities from 37.9 to 297.3 days were related to the magnetic Rossby-type waves. For cycle 23, Gachechiladze et al. (2019) found that sunspot areas revealed periodicities of 150–175, 240–270, 310–320, 370–380, and 450–460 days, which can be connected with different harmonics of global fast

magneto-Rossby waves. Knaack et al. (2005) have found a series of quasiperiodicities in the total magnetic flux of the southern hemisphere at 124–129, 151–158, 177, 209–222, 232–249, 282 ± 4, and 307–337 days, and in addition for the net flux at 100–103 days, which agree with period estimates for equatorially trapped Rossby waves with $m = 8, 10, 12, \ldots, 26$.

Oscillations $P1$ were associated with the GMF structures lasting ≈10–20 CRs. The arrows indicate changes in some of these structures and associated wave "packages." The intensity of oscillations $P1_{MF}$ and $P1_{PHOT}$ was higher in cycles 21 and 22 and it dropped dramatically in cycles 23 and 24. They match well the evolution of $S2$ and $S4$ sectorial harmonics and $S0$ GMF component. The correlation of $P1_{MF}$, $P1_{LON}$, and $P1_{PHOT}$ with Ss was 0.674, 0.638, and 0.605 and that with $S2$ ($S4$) was 0.409 (0.592), 0.472 (0.367), and 0.372 (0.512), and with $S0$ it was 0.559, 0.445, and 0.553. The oscillations include well-known Rieger (Rieger et al. 1984) and Rieger-type (Lou 2000) periodicities. Oscillations of $P1$ appeared at the maximum during the limited time intervals as separate pulses of increased intensity. For sunspot area data, Lean (1990) have also found that the periodicity of 155 days was significant during the maximum and appeared intermittently in intervals of 1–3 yr during cycles 12–21. The periodicity may drift from 130 to 180 days. In sunspot data, Gurgenashvili et al. (2016) also found a Rieger-type periodicity of 185–195 days for weak cycles and 155–165 days for strong cycles. Periods of ~51, 78, 102, 128, and 154 days revealed in various solar flare and sunspot area or group parameters during solar maxima are most likely related to large-scale equatorially trapped Rossby-type waves in the solar photosphere (Lou 2000). Comparing Figure 3 with Figure 1 in Gurgenashvili et al. (2016) shows that the onset of intensification in the periods in the range of 165–175 days in the areas of active region areas (ARAs) during 1980–1982 (Gurgenashvili et al. 2016) coincides with the intensity increase in $P1$ (CRs 1691–1717) and the formation of a four-sector GMF structure in cycle 21. In cycle 22, an increase in intensity in the range of 170–190 days during 1990–1993 (Gurgenashvili et al. 2016) coincides with an increase in the intensity of $P1$ and the formation of a two-sector structure (CRs 1825–1865). In cycle 23, an increase intensity in the range of 160–200 days in ARAs during 2000–2005 (Gurgenashvili et al. 2016) coincides with an increase in the intensity of $P1$ (CRs 1958–1980) and the formation of a two-sector structure. Many periodicities belonging to $P1$ (from ≈25 to 250 days), matching theoretical Rossby modes, were found in GOES X-ray flare data (Dimitropoulou et al. 2008).

5. Discussion and Conclusion

The GMF structures and associated oscillations during cycles 21–24 were investigated. The results indicate that GMF structures were associated with certain oscillations. The intensity of the oscillations correlated with the magnetic activity of the Sun: more intense oscillations occurred during stronger cycles. Some periodicities of the revealed oscillations are in good agreement with the estimates of the periods for fast magnetic Rossby waves (Zaqarashvili et al. 2007; Zaqarashvili 2018).

Structures lasting ≈10–20 CRs were associated with oscillations of 81.83–163.65 days. The oscillations correlated well with the sectorial harmonics $S2$ and $S4$, and the $S0$ GMF component. They appeared as pulses during solar maxima. Some of these oscillations belong to the Rieger and Rieger-type periodicities. Zaqarashvili et al. (2010a) showed that the periodicities of

155–160 days can be connected to the dynamics of magnetic Rossby waves in the upper part of the tachocline around the cycle maximum. The periods and growth rates of unstable harmonics depend on the differential rotation parameters and the magnetic-field strength. A magnetic field with a strength $\leqslant 10^4$ G leads to oscillations with a period of 150–170 days (Zaqarashvili et al. 2010b).

Oscillations of 163.652–463.680 days were associated with GMF structures lasting $\approx$20–50 CRs. They followed the two-peak magnetic-field evolution. A number of oscillations from this range are related to the magnetic Rossby waves (Knaack et al. 2005; Gachechiladze et al. 2019).

Oscillations of 1.270–5.231 yr appeared during the sectorial GMF structure domination. Zaqarashvili et al. (2010b) suggested that the unstable magnetic Rossby waves in the solar tachocline could be responsible for the observed intermediate periodicities in solar activity. A strong toroidal magnetic field with a strength $\geqslant 10^5$ G and strongly stable stratification leads to formation oscillations with periods 1–2.5 yr in the main part of the tachocline.

Oscillations of 5.231–14.945 yr had the highest intensity. From cycle 22 to 24, their intensity decreased, and the range of periods narrowed and shifted to longer periods, determining the corresponding changes in the oscillations of 81.83 days–5.231 yr and associated GMF structures. They match the evolution of the zonal GMF structure. They are assumed to be a descending part of the period of $\approx\geqslant 60$ yr. A decrease in their intensity was probably the cause of the decrease in the magnetic field from cycle 22 to 24. Zaqarashvili (2018) showed that if assuming reduced gravity, global equatorial fast magneto-Rossby waves match well the 11 yr cycles. Raphaldini & Raupp (2015) proposed the description of 11 yr cycle based on resonant nonlinear interactions among MHD Rossby waves in the solar tachocline.

ORCID iDs

Irina A. Bilenko ⬤ https://orcid.org/0000-0002-9543-0542

References

Altschuler, M. D., Levine, R. H., Stix, M., & Harvey, J. 1977, SoPh, 51, 345
Altschuler, M. D., & Newkirk, G., Jr. 1969, SoPh, 9, 131
Altschuler, M. D., Trotter, D. E., Newkirk, G., Jr., & Howard, R. 1975, SoPh, 41, 225
Bilenko, I. A. 2012, Ge&Ae, 52, 1005
Bilenko, I. A. 2013, in Proc. IAU Symp. 300, Nature of Prominences and their Role in Space Weather, ed. B. Schmieder, J.-M. Malherbe, & S. T. Wu (Cambridge: Cambridge Univ. Press), 168
Bilenko, I. A. 2014, SoPh, 289, 4209
Bilenko, I. A., & Tavastsherna, K. S. 2016, SoPh, 291, 2329
Dimitropoulou, M., Moussas, X., & Strintzi, D. 2008, MNRAS, 386, 2278
Feng, S., Yu, L., Wang, F., Deng, H., & Yang, Y. 2017, ApJ, 845, 11
Gachechiladze, T., Zaqarashvili, T. V., Gurgenashvili, E., et al. 2019, ApJ, 874, 162
Gilman, P. A. 1969a, SoPh, 8, 316
Gilman, P. A. 1969b, SoPh, 9, 3
Gurgenashvili, E., Zaqarashvili, T. V., Kukhianidze, V., et al. 2016, ApJ, 826, 55
Hoeksema, J. T. 1984, Structure and Evolution of the Large Scale Solar and Heliospheric Magnetic Fields, PhD thesis, Stanford Univ.
Hoeksema, J. T. 1991, AdSpR, 11, 15
Hoeksema, J. T., & Scherrer, P. H. 1988, AdSpR, 8, 177
Knaack, R., & Stenflo, J. O. 2005, A&A, 438, 349
Knaack, R., Stenflo, J. O., & Berdyugina, S. V. 2005, A&A, 438, 1067
Kuhn, J. R., Armstrong, J. D., Bush, R. I., & Scherrer, P. 2000, Natur, 405, 544
Lean, J. L. 1990, ApJ, 363, 718
Levine, R. H. 1977, SoPh, 54, 327
Levine, R. H. 1979, SoPh, 62, 277
Liang, Z.-C., Gizon, L., Birch, A. C., & Duvall, N. L., Jr. 2019, A&A, 626, A3
Löptien, B., Gizon, L., Birch, A. C., et al. 2018, NatAs, 2, 568
Lou, Y.-Q. 2000, ApJ, 540, 1102
Lou, Y.-Q., Wang, Y.-M., Fan, Z., Wang, S., & Wang, J. X. 2003, MNRAS, 345, 809
Mackay, D. H., & Yeates, A. R. 2012, LRSP, 9, 6
McIntosh, S. W., Cramer, W. J., Marcano, M. P., & Leamon, R. J. 2017, NatAs, 1, 0086
Mei, Y., Deng, H., & Wang, F. 2018, Ap&SS, 363, 84
Mordvinov, A. V., Salakhutdinova, I. I., Plyusnina, L. A., Makarenko, N. G., & Karimova, L. M. 2002, SoPh, 211, 241
Ponyavin, D. I. 2004, SoPh, 224, 465
Raphaldini, B., & Raupp, C. F. M. 2015, ApJ, 799, 13
Raphaldini, B., Teruya, A. S., Raupp, C. F. M., & Bustamante, M. D. 2019, ApJ, 887, 1
Rieger, E., Kanbach, G., Reppin, C., et al. 1984, Natur, 312, 623
Schatten, K. H., Wilcox, J. M., & Ness, N. F. 1969, SoPh, 6, 442
Scherrer, P. H., Wilcox, J. M., Kotov, V., Severny, A. B., & Howard, R. 1977, SoPh, 52, 3
Silva, H. G., & Lopes, I. 2017, Ap&SS, 362, 44
Stix, M. 1977, A&A, 59, 73
Sturrock, P. A., Bertello, L., Fischbach, E., et al. 2013, APh, 42, 62
Svalgaard, L., Hannah, I. G., & Hudson, H. S. 2011, ApJ, 733, 49
Tikhomolov, E. M., & Mordvinov, V. I. 1996, ApJ, 472, 389
Wang, Y. M., & Sheeley, N. R., Jr. 1994, JGR, 99, 6597
Wilcox, N. F. 1967, SoPh, 1, 437
Zaqarashvili, T. 2018, ApJ, 856, 32
Zaqarashvili, T. V., Carbonell, M., Oliver, R., & Ballester, J. L. 2010a, ApJ, 709, 749
Zaqarashvili, T. V., Carbonell, M., Oliver, R., & Ballester, J. L. 2010b, ApJL, 724, L95
Zaqarashvili, T. V., Oliver, R., Ballester, J. L., & Shergelashvili, B. M. 2007, A&A, 470, 815
Zaqarashvili, T. V., Oliver, R., Hanslmeier, A., et al. 2015, ApJL, 805, L14